Eur. Phys. J. E **17**, 403–411 (2005)
DOI 10.1140/epje/i2005-10017-7

THE EUROPEAN PHYSICAL JOURNAL E

# Light-induced instabilities driven by competing helical patterns in long-pitch cholesterics

E. Brasselet[1,a], D.O. Krimer[2,b], and L. Kramer[2†]

[1] Laboratoire de Physique UMR 5672, École Normale Supérieure de Lyon, 46 Allée d'Italie, 69364 Lyon Cedex 07, France
[2] Physikalisches Institut der Universität Bayreuth, D-95440 Bayreuth, Germany

Received 2 March 2005 /
Published online: 26 July 2005 – 

**Abstract.** We study theoretically the dynamical reorientation phenomena when a long-pitch cholesteric liquid-crystal film with homeotropic alignment is illuminated by a circularly polarized lightwave. In the present case, the natural cholesteric pitch is of the order of (or larger than) the film thickness. The helical cholesteric structure is thus frustrated by the boundary conditions without illumination. However, above a light intensity threshold reorientation occurs and the bifurcation scenario depends strongly on the natural cholesteric pitch. Recalling that a long-pitch cholesteric is achieved in practice by adding a small amount of chiral agents in a nematic liquid crystal, the observed dynamics can be viewed as the result of the competition between intrinsic and extrinsic unidimensional helical patterns. The intrinsic part consists of the helical deformations induced by the chirality of the dopant, whereas the extrinsic part is related to the chirality induced by the optical field through the non-uniform angular momentum transfer of light to a nematic. The all-optical analog in the case of a pure nematic (without chiral dopant), is also discussed.

**PACS.** 42.70.Df Liquid crystals – 42.65.Sf Dynamics of nonlinear optical systems; optical instabilities, optical chaos and complexity, and optical spatio-temporal dynamics

## 1 Introduction

By doping a nematic liquid crystal with chiral molecules a cholesteric phase is induced which supports a unidimensional helical structure of the director profile [1]. This helical structure is characterized by a pitch $P$ or the wave vector $q = 2\pi/P$ that can be of both signs distinguishing between right- and left-handed helices. These mixtures have been widely used in the realization of twisted cells for liquid-crystal displays that are usually made in planar alignment. For this reason, only a few studies were devoted to the case of homeotropic alignment which is nevertheless interesting because of the incompatibility between a bulk homeotropic alignment and the helix formation. In fact, the bulk homeotropic orientation is stable for small enough values of $|q|$ while it is unstable above a threshold value, $q = q^*$, where a helix structure appears. In spatially extended systems this leads to the formation of twisted domains which can be eventually quenched by applying a suitable electric field [2,3].

In [4–6] the reorientation of the director induced by polarized light impinging at normal incidence onto a long-pitch cholesteric ($|q| < q^*$) sample with homeotropic anchoring conditions has been studied. There, the liquid crystal was a mixture of a nematic liquid crystal with a small quantity of a cholesteric one. It was shown that the initial homeotropic alignment is unstable above a light intensity threshold value, $I = I_{\rm th}$, where the optical Fréedericksz transition (OFT) takes place as in the pure nematic case ($q = 0$). The observed dependence of $I_{\rm th}$ as a function of $q$ has confirmed the prediction that the OFT threshold value is decreased in comparison to the case $q = 0$ and that such a decrease is insensitive to the sign of $q$, as expected. Moreover, the nature of the OFT was found experimentally to differ qualitatively from the case of a pure nematic.

In the case of linear polarized light, the OFT turns out to be continuous as in the case of a pure nematic. However, contrary to the pure case, a discontinuous transition to a largely reoriented state, which is accompanied with a large hysteresis, was observed at some higher intensities [4, 5]. This effect was also observed when the incident light is circularly polarized [6], however, the reorientation was demonstrated to depend significantly on the relative helicity of the light field and the chiral mixture. Denoting by $\sigma_+$ [$\sigma_-$] the case of a circular polarization with same [opposite] helicity to the one of the material, one can state for

[a] e-mail: ebrassel@ens-lyon.fr
[b] e-mail: Dmitry.Krimer@uni-bayreuth.de
[†] Deceased.

instance the two following points: i) a large optical bistability is observed for the $\sigma_+$ situation when $|q|$ is large enough; ii) the reorientation for $\sigma_-$ is similar to the one of linear polarized light with $q = 0$ [6]. Whereas the dependence of the threshold for OFT *versus* chiral dopant concentration and the optical phase locking (OPL, which refers to the fact that the optically induced birefringence remains about $\pi$ [5] over a relatively wide range of intensities above the OFT) were correctly described, the model presented failed to reproduce the other observations [6].

In the present paper, we consider the detailed theoretical study of the optical reorientation induced by circularly polarized light in long-pitch cholesterics, *i.e.* chirally doped nematics. The competition between an *intrinsic* (owing to the chiral dopant) and an *extrinsic* (owing to the light [7]) helical pattern is shown to be at the origin of a complex behavior. The qualitatively different bifurcation scenarios that have been previously observed for right- and left-handed circular polarizations are fully described. In addition, different kinds of bifurcation scenarios are quantitatively predicted depending on the actual value of $q$, when the light intensity is regarded as a control parameter. Moreover, some dynamical regimes that have not been reported yet are predicted and a possible experimental observation of such regimes is proposed.

We first present a stationary model that describes the OFT assuming a time-independent spatial configuration of the reoriented liquid crystal, which allows for the uniform precession of the director [8]. The nature of the OFT is shown to be discontinuous or continuous and optical bistability can occur *in its neighborhood* depending on the actual twisting power of the sample. Such predictions are further confirmed by a dynamical model that, in addition, allows us to describe more complex behaviors such as the nutation-precession motion of the director [9]. All the observations that have been reported so far both for the $\sigma_+$ and $\sigma_-$ cases are quantitatively described. For instance, the nature of the bifurcation to a large reoriented state, the intermediate dynamical regimes and instabilities experienced by the system are demonstrated to depend strongly on $q$. Finally, we compare the situation with its all-optical analog (without chiral dopant) in the case of a pure nematic, where the excitation optical field is obtained from the superposition of two incoherent circularly polarized beams carrying identical or opposite angular momentum.

The description of the optically induced reorientation involves the dynamics of the director $\boldsymbol{n} = (\sin\Theta\cos\Phi, \sin\Theta\sin\Phi, \cos\Theta)$ that designates the local optical axis orientation in a Cartesian coordinate system $(x, y, z)$ with the $z$-axis along the direction of the wave vector of light and $(\Theta, \Phi)$ being the usual spherical angles. The treatment is developed in the infinite plane-wave approximation, justified experimentally if the spot size of the excitation beam is significantly larger than the thickness $L$ of the film. Under this assumption, all the relevant functions depend solely on the spatial coordinate $z$ and the time $t$. The theory presented here consists of the straightforward extension of the known theory developed for the pure nematic, to which we will refer from now on by the superscript "$N$". To generalize to a chiral nematic case one has to add a chiral part to the elastic free energy density

$$F_{\rm el} = F_{\rm el}^{(N)} + qK_2(\boldsymbol{n}\cdot\boldsymbol{\nabla}\times\boldsymbol{n})\,. \tag{1}$$

Then, the intrinsic helical structure induced by the chiral dopant is taken into account by writing the twist angle $\Phi$ as

$$\Phi(z,t) = \Phi^{(N)}(z,t) + k_2 q z\,, \tag{2}$$

where $k_2 = K_2/K_3$ and $K_i$ are the Franck elastic constants. The strong homeotropic anchoring conditions are written $\Theta(0,t) = \Theta(L,t) = 0$ and $\partial_z\Phi(0,t) = \partial_z\Phi(L,t) = k_2 q$ (note that $\partial_z\Phi^{(N)}(0,t) = \partial_z\Phi^{(N)}(L,t) = 0$, see for instance [10]).

In the calculations, we took the material parameters for the nematic E7, as in the experiments [4–6]: $K_1 = 11.09\times10^{-12}$ N, $K_2 = 5.82\times10^{-12}$ N, $K_3 = 15.97\times10^{-12}$ N [11], $n_e = 1.746$, $n_o = 1.522$ [12] (extraordinary and ordinary refractive indices), $\gamma_1/K_3 = 10^{10}$ s m$^{-2}$ [13], where $\gamma_1$ is the rotational viscosity. Following the experimental conditions [6] the thickness of the liquid-crystal film and the wavelength of the laser are taken to be $L = 50$ $\mu$m and $\lambda = 514.5$ nm, respectively. We also introduced the characteristic relaxation time of the director $\tau_{\rm NLC} = \gamma_1 L^2/\pi^2 K_3$. In what follows, without loss of generality, the incident light is chosen to be a left-handed circularly polarized helix propagating towards $z > 0$. Thus, $q > 0$ corresponds to the $\sigma_-$ case and $q < 0$ to the $\sigma_+$ one.

## 2 Theoretical model

The dynamical equations of motion for the angles $\Theta$ and $\Phi$ are obtained from the balance of torques (elastic, electromagnetic and viscous) acting on the nematic. In the absence of a velocity field they can be written as

$$\frac{\partial\Theta}{\partial\tau} = \mathcal{L}_\Theta^{(N)} + \mathcal{L}_\Theta^*(q)\,, \tag{3}$$

$$\frac{\partial\Phi}{\partial\tau} = \mathcal{L}_\Phi^{(N)} + \mathcal{L}_\Phi^*(q)\,, \tag{4}$$

where time $\tau$ is normalized to $\tau_{\rm NLC}$. The expressions of the torques $\mathcal{L}_\Theta^{(N)}$ and $\mathcal{L}_\Phi^{(N)}$ for pure nematic can be found in [9]. The torques $\mathcal{L}_\Theta^*$ and $\mathcal{L}_\Phi^*$ are obtained by calculating the corresponding variational derivatives of the chiral part of the elastic free energy (see Eq. (1))

$$\mathcal{L}_\Theta^* = \widetilde{q}\,k_2\sin2\Theta\Big\{\widetilde{q}\,k_2\left[1/2 + (1-k_2)\sin^2\Theta\right] + 2(1-k_2)\sin^2\Theta\left(\frac{1}{\pi}\frac{\partial\Phi^{(N)}}{\partial\xi}\right)\Big\}\,, \tag{5}$$

$$\mathcal{L}_\Phi^* = -2\widetilde{q}k_2(1-k_2)\sin2\Theta\left(\frac{1}{\pi}\frac{\partial\Theta}{\partial\xi}\right)\,, \tag{6}$$

where the length is normalized according to $\xi = z/L$ and $\widetilde{q} = qL/\pi$ is the normalized chiral parameter.

Following the methods presented in [9] for the pure nematic case, we expand $\Theta$ and $\Phi^{(N)}$ with respect to $\xi$ in systems of orthogonal functions which satisfy the boundary conditions, namely

$$\Theta(\xi,\tau) = \sum_{n=1}^{\infty} \Theta_n(\tau)\sin(n\pi\xi)\,, \tag{7}$$

$$\Phi^{(N)}(\xi,\tau) = \Phi_0(\tau) + \sum_{n=1}^{\infty} \Phi_n(\tau)\frac{\sin[(n+1)\pi\xi]}{\sin(\pi\xi)}. \tag{8}$$

In equation (8) the zeroth mode $\Phi_0(\tau)$ does not depend on $\xi$ and describes a rigid rotation of the director (without elastic distortion) around the $z$-axis.

After substituting these expansions into equations (3, 4) with further projection of equation (3) onto the modes $\Theta_n$ and equation (4) onto $\Phi_n$ (Galerkin method), a set of coupled nonlinear ODEs for the modes $\Theta_n$ and $\Phi_n$ is obtained

$$\frac{\mathrm{d}\Theta_n}{\mathrm{d}\tau} = 2\int_0^1 \left[\mathcal{L}_\Theta^{(N)} + \mathcal{L}_\Theta^*\right]\sin(n\pi\xi)\mathrm{d}\xi\,, \tag{9}$$

$$\frac{\mathrm{d}\Phi_n}{\mathrm{d}\tau} = 2\int_0^1 \left[\mathcal{L}_\Phi^{(N)} + \mathcal{L}_\Phi^*\right]\sin[(n+1)\pi\xi]\sin(\pi\xi)\mathrm{d}\xi. \tag{10}$$

The infinite set of ODEs given by equations (9, 10) was truncated and solved by the Runge-Kutta method together with the equations that govern the propagation of light inside the nematic (see [9] for details). One retains a sufficient number of modes to ensure convergence of the results within a given tolerance. It should be noted that since the chirality does not break the rotational symmetry, the ODE for $\Phi_0(\tau)$ is decoupled from the rest as in the case of a pure nematic.

When $\Theta_n$ and $\Phi_{n\geq 1}$ do not depend on time [$\mathrm{d}\Theta_n/\mathrm{d}\tau = \Phi_{n\geq 1}/\mathrm{d}\tau = 0$], the director precesses uniformly around the $z$-axis with a constant normalized angular velocity $\Omega$ defined as $\Omega = \mathrm{d}\Phi_0/\mathrm{d}\tau$. In this case, the problem is significantly simplified. In fact, instead of solving a system of evolution equations for $\Phi_n(\tau)$ and $\Theta_n(\tau)$, we are now faced with a set of nonlinear algebraic equations. After solving them by a Newton-Raphson method and substituting $\Phi_n$ and $\Theta_n$ into the equation for $\Phi_0$, the angular velocity $\Omega$ of the uniform precession can be found. We call such a state a uniform precession (UP) state. Moreover, the linear stability analysis of a UP state can be performed by calculating the eigenvalues of the Jacobian matrix of equations (9, 10).

The other possible situation is when $\Theta_n$ and $\Phi_{n\geq 1}$ do depend on $\tau$ and thus $\mathrm{d}\Phi_0/\mathrm{d}\tau \neq$ const. Such a state corresponds to a non-uniform precession (NUP) of the director.

## 3 Approximate solution for the uniform precession states

The straightforward generalization of the approximate model developed in [10] for the UP states prompts us to write the angles $\Theta$ and $\Phi$ as

$$\Theta = \Theta_1\sin(\pi\xi)\,, \tag{11}$$

$$\Phi = \Omega\tau + \alpha(\xi) + k_2\widetilde{q}\,\pi\xi\,, \tag{12}$$

where $\Theta_1$ is the amplitude of the polar angle $\Theta$ to lowest order (see Eq. (7)). The expression for the constant precession rate $\Omega$ and the twist reorientation profile $\alpha(\xi)$ are identical to those for the pure nematic case (see Eqs. (65, 66) of [10]; note that there $\alpha$ is denoted by $\varphi$), which were obtained assuming smallness of both the polar angle ($\Theta^2 \ll 1$) and the twist distortion ($|\,\partial\alpha/\partial\xi| < 1$). We introduce the phase delay between the extraordinary and the ordinary wave $\Delta = (2\pi/\lambda)\int_0^1 [n_e(\xi) - n_o]\,\mathrm{d}\xi$, where $n_e(\xi) = n_e n_o/(n_e^2\cos^2\Theta + n_o^2\sin^2\Theta)^{1/2}$, which depends on $\Theta$ only and is a global measure of the amplitude of reorientation. Within the given approximation, $\Delta$ is related to the reorientation amplitude $\Theta_1$ as $\Delta = \widetilde{L}\Theta_1^2$. Here $\widetilde{L} = L\pi n_o(n_e^2 - n_o^2)/(2n_e^2\lambda)$ is a normalized cell thickness. The condition $\Theta^2 \ll 1$ thus implies $\Delta \ll \widetilde{L}$, where $\widetilde{L} = 55.8$ in the present situation. Using the additional assumption that $|\,k_2\widetilde{q}| < 1$, the following approximate transcendental equation for the phase delay $\Delta$ can been derived

$$\Delta\,\left[a(\Delta)\rho^2 - b(\Delta,\widetilde{q})\rho + c(\Delta,\widetilde{q})\right] = 0\,, \tag{13}$$

where

$$a(\Delta) = \frac{\pi^2}{2}\int_0^1 \Big\{\Psi^2(\xi)\sin^2(\pi\xi) - 2[1-u(\xi)]\Psi(\xi)\sin[\Delta u(\xi)]\Big\}\mathrm{d}\xi\,, \tag{14}$$

$$b(\Delta,\widetilde{q}) = 1 - \frac{\mu}{\widetilde{L}}\,\Delta + 2\pi\widetilde{q}\,k_2\int_0^1 [1-u(\xi)]\sin[\Delta u(\xi)]\,\mathrm{d}\xi\,, \tag{15}$$

$$c(\Delta,\widetilde{q}) = 1 - \widetilde{q}^{\,2}k_2^2 - \frac{1-k_1}{2\widetilde{L}}\,\Delta\,, \tag{16}$$

and

$$\Psi(\xi) = \frac{1}{\Delta\sin^2(\pi\xi)}\left[(1-\cos\Delta)u(\xi) + \cos[\Delta u(\xi)] - 1\right]\,, \tag{17}$$

with $u(\xi) = \xi - \sin(2\pi\xi)/(2\pi)$. Here $\rho = I/I_{\mathrm{th}}^{(N)}$ is the normalized light intensity and $I_{\mathrm{th}}^{(N)}$ is the OFT threshold intensity for $\widetilde{q} = 0$. In equation (15) $\mu = (9\varepsilon_\perp - 5\varepsilon_\parallel)/(8\varepsilon_\parallel)$, where $\varepsilon_\perp = n_o^2$ ($\varepsilon_\parallel = n_e^2$) is the dielectric permittivity, at optical frequency, perpendicular (parallel) to $\boldsymbol{n}$. It will turn out that even if the condition $\Theta^2 \ll 1$ is not satisfied (*i.e.* when $\Delta \sim \widetilde{L}$, which corresponds to the case of large reorientation of the director) the approximate model still captures the main features of the UP solution.

It can be shown from the linearized equations (13–17) that the director is unperturbed until the intensity reaches the threshold value

$$\rho_{\mathrm{th}}(\widetilde{q}) = 1 - \widetilde{q}^{\,2}k_2^2\,, \tag{18}$$

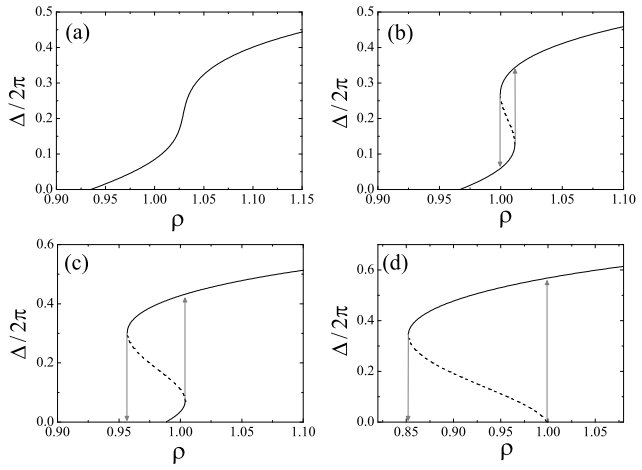


**Fig. 1.** $\Delta/2\pi$ *versus* $\rho$ in the neighborhood of the optical Fréedericksz transition calculated from the approximate model for $\widetilde{q} = -0.7$ (a), $\widetilde{q} = -0.5$ (b), $\widetilde{q} = -0.3$ (c) and $\widetilde{q} = 0.1$ (d). The solid (dashed) lines are stable (unstable) states.

Note that for $\widetilde{q} > \widetilde{q}^* = 1/k_2 \simeq 2.74$ the homeotropic alignment $\boldsymbol{n} = (0, 0, 1)$ is destabilized in favor of a twisted structure already without light [14]. The lowering of the OFT in the presence of a chiral dopant agrees with previous work where a linearized theory was used [6] but, in addition, the present approximate model captures the stationary nonlinear behavior above the OFT. Thus, from equation (13) one finds that the OFT can be continuous (when $\widetilde{q} < \widetilde{q}_c$) or discontinuous (when $\widetilde{q} > \widetilde{q}_c$) with the critical value

$$\widetilde{q}_c = \frac{6\pi(2\mu - 1 + k_1)}{k_2 \widetilde{L}(4\pi^2 - 15)}\,. \tag{19}$$

In the present case we found that $\widetilde{q}_c \simeq 5.8 \times 10^{-3}$. In Figure 1 panels (a-c) correspond to $\widetilde{q} < \widetilde{q}_c$ and panel (d) corresponds to $\widetilde{q} > \widetilde{q}_c$. When the transition is continuous ($\widetilde{q} < \widetilde{q}_c$) a subsequent discontinuous transition with hysteresis takes place for $\widetilde{q}_h < \widetilde{q} < \widetilde{q}_c$ as illustrated by Figures 1(b, c). The value $\widetilde{q}_h$, above which optical bistability occurs, is determined by the conditions $\partial_\Delta \rho|_{\Delta=\Delta_h} = 0$ and $\partial^2_\Delta \rho|_{\Delta=\Delta_h} = 0$, where $\Delta = \Delta_h$ is the phase delay that corresponds to the birth of the hysteresis loop. Such conditions can be rewritten as (neglecting the terms proportional to $1/\widetilde{L}$ with respect to the terms of the order of 1)

$$\partial_\Delta a\,(\Delta_h)\,\partial^2_\Delta b\,(\Delta_h, \widetilde{q}_h) = \partial^2_\Delta a\,(\Delta_h)\,\partial_\Delta b\,(\Delta_h, \widetilde{q}_h)\,, \tag{20}$$

that gives $\widetilde{q}_h \simeq -0.63$ and $\Delta_h \simeq 1.29$. Moreover, in the hysteretic region, reoriented states can exist for $\rho < \rho_{\rm th}$ if $\widetilde{q} > -0.40$ as illustrated by Figure 1(c). Another feature of the model is the OPL around $\Delta \simeq \pi$ which is clearly observed for $\widetilde{q} \leq 0$, as illustrated by Figure 2(a–c) where the reorientation diagram is plotted over a larger range of intensities for different values of $\widetilde{q}$.

In summary, the stationary approximate model describes the main features both in $\sigma_+$ and $\sigma_-$ geometries at small reorientation amplitude. However, the discontinuous transition to a largely reoriented state in the $\sigma_+$ case is not predicted although this state is correctly described

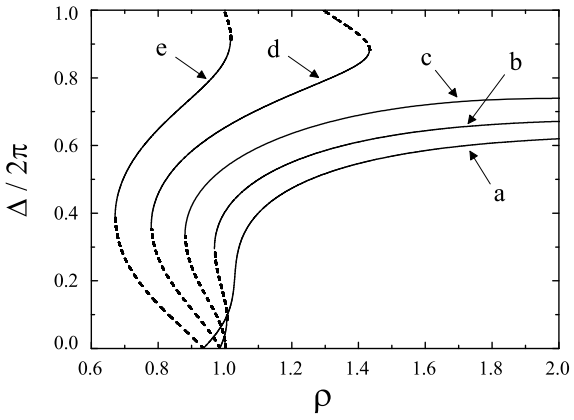


**Fig. 2.** $\Delta/2\pi$ *versus* $\rho$ (approximate model) for $\widetilde{q} = -0.7$ (a), $\widetilde{q} = -0.35$ (b), $\widetilde{q} = 0$ (c), $\widetilde{q} = 0.35$ (d) and $\widetilde{q} = 0.7$ (e). The solid (dashed) lines are stable (unstable) states.

(not visible on the scale of Fig. 2). In fact, a rigorous treatment is required to describe properly the director dynamics. Results of numerical simulations are presented in the next section.

## 4 Numerical simulations

We simulated the director dynamics from the set of equations governing the behavior of the system as explained at the end of Section 2 and found various bifurcation scenarios depending on $\widetilde{q}$. The result is shown in Figure 3 where solid (dashed) lines correspond to stable (unstable) UP states and the gray regions correspond to NUP states. As was already mentioned, the UP state (NUP state) is characterized by a time-independent (time-dependent) amplitude of the spatial reorientation modes and precession angular velocity (see Eqs. (7, 8)). The phase delay $\Delta$ thus depends on time only for NUP state via $\Theta(\xi, \tau)$ so that the gray region in Figure 3 represents the range of values explored by $\Delta(\tau)$. It turns out that NUP states exist only in a finite window of the chiral parameter $\widetilde{q}_1 < \widetilde{q} < \widetilde{q}_2$, where $\widetilde{q}_1 \simeq -1.17$ and $\widetilde{q}_2 \simeq 0.53$. The bifurcation scenarios outside and inside this window are discussed separately in what follows. We refer the reader to [9,15] for a detailed description of the different regimes and transitions between them for the pure case $\widetilde{q} = 0$.

### 4.1 Large chiral doping ($\widetilde{q} < \widetilde{q}_1$ or $\widetilde{q} > \widetilde{q}_2$)

The typical scenarios for $\widetilde{q} < \widetilde{q}_1$ and $\widetilde{q} > \widetilde{q}_2$ are shown in Figures 3(a, d), respectively. As one sees from Figure 3(a), where $\widetilde{q} = -1.235$, OPL takes place approximately for $1.25 < \rho < 2.0$. On the contrary, for $\widetilde{q} > \widetilde{q}_2$, OPL does not occur as illustrated by Figure 3(d) where $\widetilde{q} = 0.7$. If one starts from the UP state above the OFT and the intensity $\rho$ is increased, a discontinuous transition to a largely reoriented state with hysteresis takes place in both cases, but for $\widetilde{q} < \widetilde{q}_1$ the hysteretic loop is much wider.

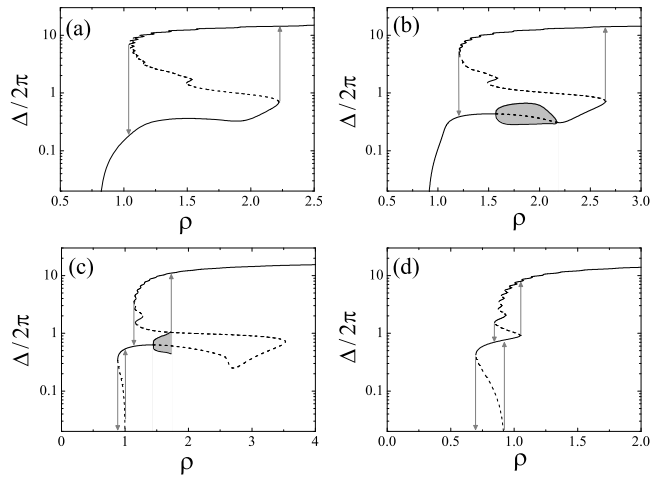


**Fig. 3.** $\Delta/2\pi$ *versus* $\rho$ (simulations) in semi-logarithmic scale for $\widetilde{q} = -1.235$ (a), $\widetilde{q} = -0.9$ (b), $\widetilde{q} = 0$ (c) and $\widetilde{q} = 0.7$ (d). The solid (dashed) lines are stable (unstable) states and the gray regions refer to precession-nutation regimes.

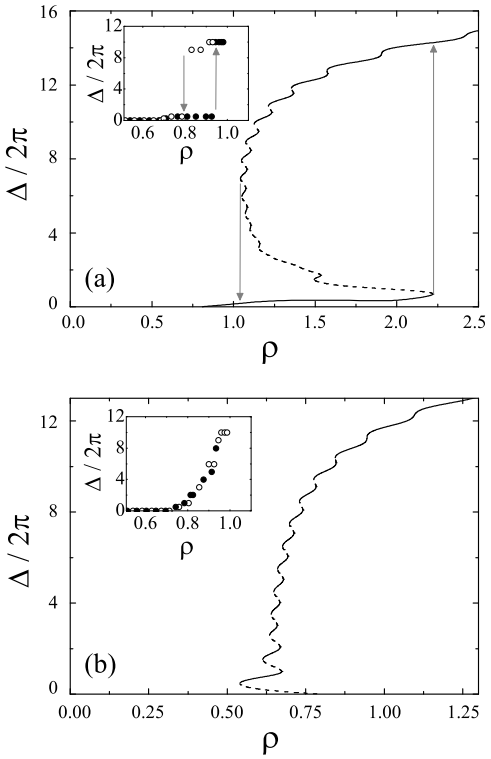


**Fig. 4.** Comparison between experiment and theory with $\widetilde{q} = -1.235$ [$\sigma_+$ geometry] (a) and $\widetilde{q} = 1.235$ [$\sigma_-$ geometry] (b). The insets are experimental figures taken from [6] where • refers to increasing intensity and ∘ refers to decreasing intensity. The simulations are performed for the same parameters. The solid (dashed) lines are stable (unstable) states.

In fact, these results describe qualitatively the observations reported in [6] both for the $\sigma_+$ and $\sigma_-$ geometries. More precisely, the comparison between experiment and theory is shown in Figure 4 where the simulations are performed for the values $\widetilde{q} = \pm 1.235$ that correspond to the experimental conditions reported in [6]. Only qualitative satisfactory agreement is found between theory and experiment. Indeed, the thresholds are quite different. The reason for that could be, for instance, the use of a finite beam size in the experiment whereas in the theory the infinite plane-wave approximation has been assumed. In addition, we notice that the NUP states were not observed in [6], as expected, since the experimental values of $\widetilde{q}$ are outside the interval $[\widetilde{q}_1, \widetilde{q}_2]$.

An interpretation of the characteristic features presented above can be done by considering the competition between the intrinsic helical pattern induced by the chiral dopant with the one generated by the light due to the non-uniform angular-momentum transfer to the medium [7]. In Figure 5 the intensity dependence of the phase delay $\Delta$ and other properties are depicted for $\widetilde{q} = -0.7$, 0 and 0.7. From panels (a) we see that OPL exists only for $\widetilde{q} = -0.7$ and 0 in contrast to the case $\widetilde{q} = 0.7$. However, the light-induced modifications of the overall twist distortion profile is qualitatively the same in all cases. Indeed, the light-induced part of $\Phi|_{\xi=1} - \Phi|_{\xi=0}$ becomes more negative when increasing the intensity as shown by panels (b) of Figure 5 where the dashed lines are the intrinsic contributions to the total twist profile, namely $k_2 \widetilde{q}\, \pi \xi$. Consequently, the light angular-momentum deposition tends to compensate the intrinsic torsion arising from the chiral dopant when $\widetilde{q} > 0$. This can eventually lead to unwinding of the intrinsic helical structure. The unwinding condition can be written as $q_{\rm tot} = 2\pi/P_{\rm tot} = 0$, where $P_{\rm tot} = P_{\rm intrinsic} + P_{\rm light}$ with $P_{\rm intrinsic} = 2L/(k_2\widetilde{q})$ (see Eq. (2) taking $\Phi^{(N)} \equiv 0$) and $P_{\rm light} = 2\pi L/\left(\Phi^{(N)}|_{\xi=1} - \Phi^{(N)}|_{\xi=0}\right)$. Such an unwinding effect is illustrated in panel (b3) of Figure 5. However, it is important to note that the underlying physical mechanism responsible for the existence of OPL is not the presence or absence of the unwinding process. This is demonstrated in Figure 6 where the normalized wave vector $\widetilde{q}_{\rm tot} = q_{\rm tot} L/\pi$ is plotted as a function of the intensity for different values of $\widetilde{q}$, *i.e.* the chiral dopant concentration (the curves correspond to UP states for small reorientation). From this figure, one can see that two kinds of qualitative behavior are represented by the families of curves (a–c) and (d–i), respectively. In fact, these families are defined by the condition $\widetilde{q} < \widetilde{q}_2$ and $\widetilde{q} > \widetilde{q}_2$, respectively, as depicted in the inset of Figure 6, which shows the reorientation diagram for values of $\widetilde{q}$ slightly below ($\widetilde{q} = 0.5$ for the curve (c)) and above ($\widetilde{q} = 0.55$ for the curve (d)) $\widetilde{q}_2 = 0.53$. Obviously $\widetilde{q} = \widetilde{q}_2$ can thus be viewed as a threshold-like value for the appearance of OPL. In fact, we would like to mention that the energy exchange between the ordinary ($o$) and the extraordinary ($e$) waves due to the non-adiabatic light propagation through the twisted optically anisotropic liquid crystal can be taken as an interesting indicator for the presence of OPL. For convenience, we introduce the normalized intensities of the $o$- and $e$-waves averaged along the $z$-axis in the liquid-crystal film, which are defined as $\langle |A_{o/e}|^2 \rangle = \int_0^1 |A_{o/e}(\xi)|^2 {\rm d}\xi$. Here $A_{o/e}$ are the normalized amplitudes for the $o/e$-waves inside the sample. In the absence of reorientation,

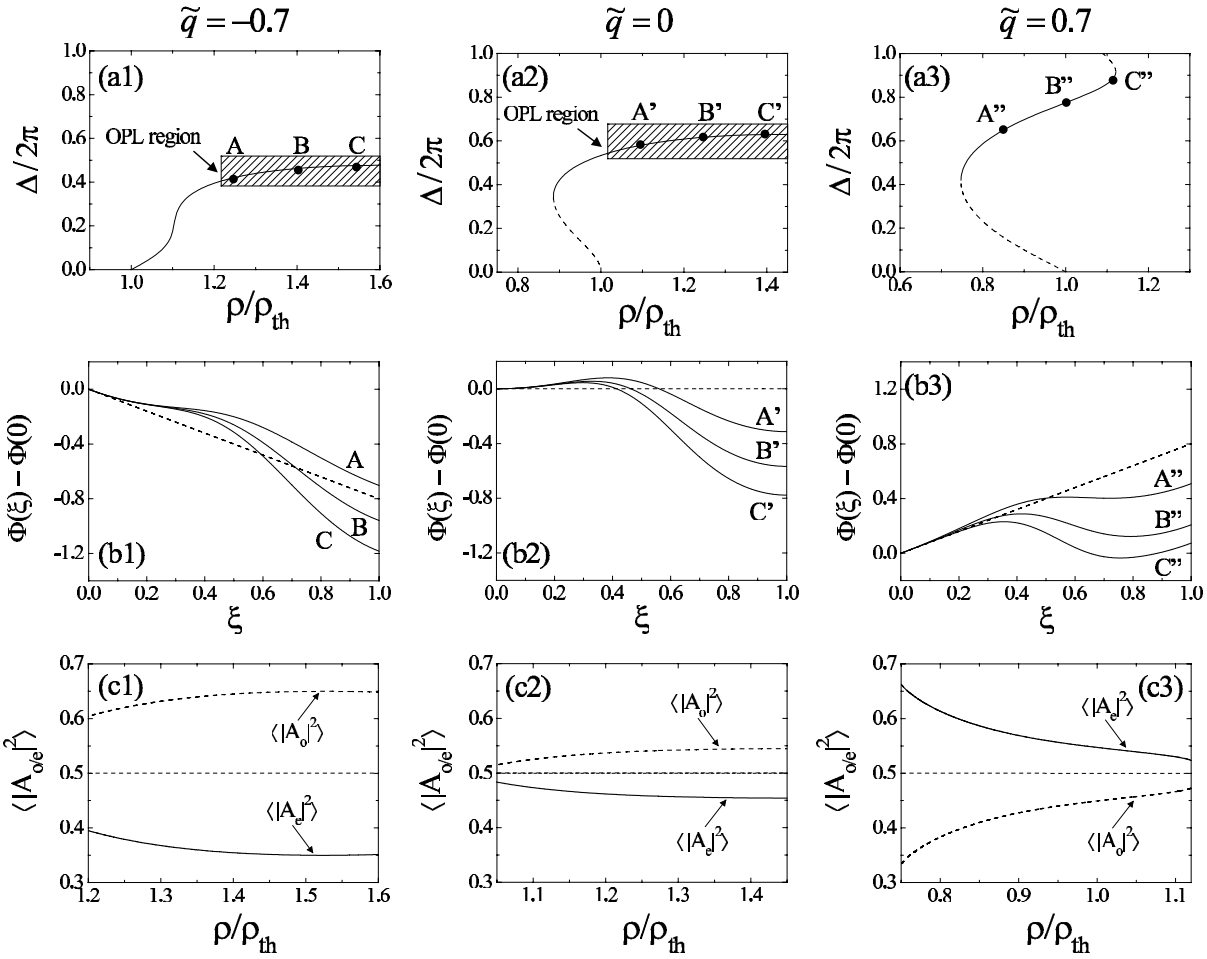


**Fig. 5.** $\Delta/2\pi$ *versus* $\rho/\rho_{\rm th}$ (first row), twist reorientation profile $\Phi(\xi)-\Phi(0)$ *versus* $\xi$ (second row) and the normalized intensities of the *e*- and *o*-waves averaged along the *z*-axis inside the liquid-crystal film, $\langle |A_{e/o}|^2 \rangle$, *versus* $\rho/\rho_{\rm th}$ (third row) for different values of $\widetilde{q}$. Left column: $\widetilde{q} = -0.7$; Center column $\widetilde{q} = 0$; Right column $\widetilde{q} = 0.7$. The dashed lines in panels (b1, b2, b3) correspond to the intrinsic contribution to the twist reorientation profile which is given by $k_2 \widetilde{q}\, \pi \xi$.

where the light remains circularly polarized during its propagation, we have $\langle |A_o|^2 \rangle = \langle |A_e|^2 \rangle = 1/2$. In Figures 5(c1, c2, c3) the quantities $\langle |A_{o/e}|^2 \rangle$ as a function of the incident intensity are shown. As one can see from Figures 5(c1, c2) the situations with OPL are characterized by $\langle |A_e|^2 \rangle < \langle |A_o|^2 \rangle$. On the contrary, $\langle |A_e|^2 \rangle > \langle |A_o|^2 \rangle$ in the absence of OPL (see Fig. 5(c3)). In other words, the twisted deformations are responsible for a self-optical limitation (amplification) of the *e*-wave's intensity in the presence (absence) of OPL. Finally, one should keep in mind that OPL is actually linked to twist reorientation which plays a role both in the elastic and optical contributions of the total torque exerted onto the director (see the appendix of [9] for the expression of these torques).

The competition between intrinsic/extrinsic helical patterns is also useful for understanding the observations in the case when the exciting light field is obtained from the superposition of two incoherent circularly polarized beams incident from opposite sides and carrying identical or opposite angular momentum in a pure nematic film [16]. In that case, the chirality of the helical patterns induced by each exciting beam separately have same sign (*i.e.* op-

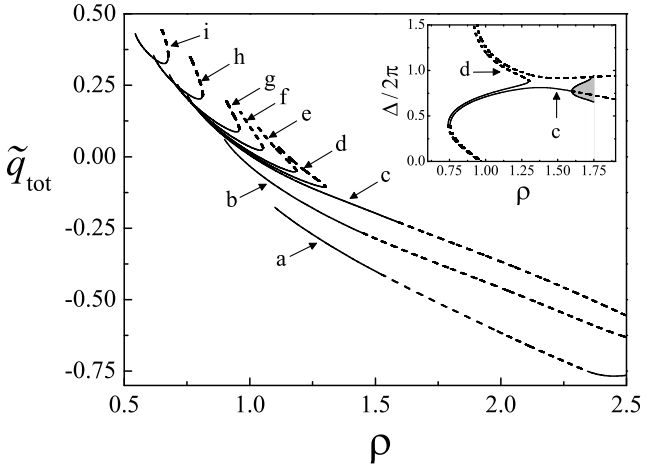


**Fig. 6.** $\widetilde{q}_{\rm tot}$ *versus* $\rho$ (simulations) for $\widetilde{q} = -0.7$ (a), $\widetilde{q} = 0$ (b), $\widetilde{q} = 0.5$ (c), $\widetilde{q} = 0.55$ (d), $\widetilde{q} = 0.6$ (e), $\widetilde{q} = 0.7$ (f), $\widetilde{q} = 0.8$ (g), $\widetilde{q} = 1$ (h) and $\widetilde{q} = 1.235$ (i). Inset: $\Delta/2\pi$ *versus* $\rho$ (simulations) for $\widetilde{q} = 0.5$ (c) and $\widetilde{q} = 0.55$ (d). The solid (dashed) lines are stable (unstable) states and the gray region refer to precession-nutation regimes.

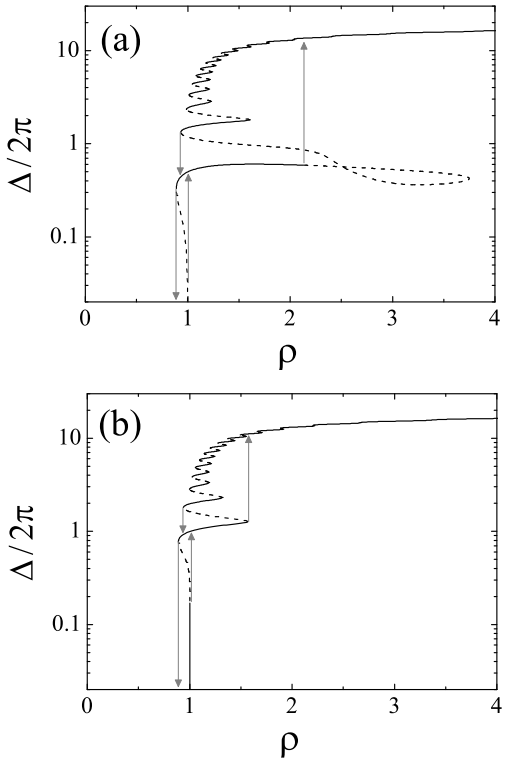


**Fig. 7.** All-optical analog with the situation when $\widetilde{q} < \widetilde{q}_1$ (a) and $\widetilde{q} > \widetilde{q}_2$ (b). Panel (a) [(b)] corresponds to the $\sigma_-$ [$\sigma_+$] geometry.

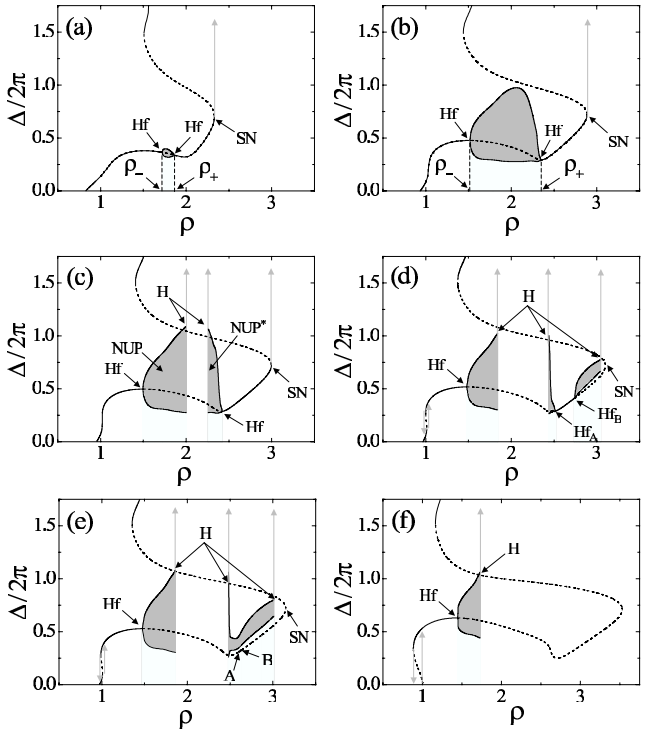


**Fig. 8.** $\Delta/2\pi$ *versus* $\rho$ (simulations) in semi-logarithmic scale for different values of $\widetilde{q}$. (a) $\widetilde{q} = -1.15$; (b) $\widetilde{q} = -0.7$; (c) $\widetilde{q} = -0.6$; (d) $\widetilde{q} = -0.5$; (e) $\widetilde{q} = -0.45$; (f) $\widetilde{q} = 0$. The solid (dashed) lines are stable (unstable) states and the gray regions refer to precession-nutation regimes. Hf, H and SN refer, respectively, to Hopf, homoclinic and saddle-node bifurcations.

posite angular momentum) or opposite sign (*i.e.* identical angular momentum). Such a situation is presented in Figures 7(a, b), which can be viewed as the all-optical analog (there is no chiral dopant) of Figures 3(a, d), respectively. As it is seen from Figure 7 the OFT threshold is $\rho_{\rm th} = 1$ as in the pure nematic under a single circularly polarized excitation (note that the total incident intensity is now defined as the sum of the intensities of the two beams) because the OFT is insensitive to the propagation direction (towards $z > 0$ or $z < 0$) and the handedness of a polarized light beam.

### 4.2 Small chiral doping ($\widetilde{q}_1 < \widetilde{q} < \widetilde{q}_2$)

For $\widetilde{q}_1 < \widetilde{q} < \widetilde{q}_2$ there are one or even more intervals of $\rho$ where the NUP states exist. In fact, we found two different kinds of scenario when the intensity is smoothly increased starting from the homeotropic state. The sequence of regimes turns out to be UP1 → NUP → UP1 → UP2 for $\widetilde{q}_1 < \widetilde{q} < -0.63$ (see Fig. 3(b)), whereas it is UP1 → NUP → UP2 for $-0.63 < \widetilde{q} < \widetilde{q}_2$ (see Fig. 3(c)). Here UP1 and UP2 states refer, respectively, to UP states with a small ($\Delta \sim \pi$) and large ($\Delta/2\pi \sim 10$) reorientation of the director. However, for $-0.63 < \widetilde{q} < -0.25$, the NUP states exist also at some higher values of $\rho$. Such states are thus not accessible by the commonly used experimental procedure which consists in a smooth increase of the intensity starting from zero. In what follows we review all possible scenarios starting from $\widetilde{q} = \widetilde{q}_1$.

Above $\widetilde{q} = \widetilde{q}_1$ the NUP states appear. They are located in a finite range of intensity $\rho_- < \rho < \rho_+$ for $\widetilde{q}_1 < \widetilde{q} < -0.63$ (Figs. 8(a, b)). The transitions UP → NUP at $\rho = \rho_-$ and $\rho = \rho_+$ are identified as supercritical Hopf bifurcations (Hf). For such values of $\widetilde{q}$ the amplitude of the limit cycle associated with the nutation motion, $\mathcal{A} = \max_\tau \Delta(\tau) - \min_\tau \Delta(\tau)$, passes through a maximum value for an intensity between $\rho_-$ and $\rho_+$ (Figs. 8(a, b)). Both, the range of intensity $\rho_+ - \rho_-$ and the maximum of $\mathcal{A}$ increase when $\widetilde{q}$ is increased from $\widetilde{q}_1$ until, at $\widetilde{q} \simeq -0.63$, the nutation limit cycle (NUP) collides with the unstable UP branch located at $\Delta/2\pi \sim 1$, which is found to be a saddle. As a result of such a collision a discontinuous transition from the NUP to the UP2 state via a homoclinic bifurcation occurs (H). On the other hand, for $\widetilde{q}_1 < \widetilde{q} < -0.63$, the discontinuous transition to the UP2 state takes place directly from the UP1 via a saddle-node bifurcation (SN) at $\rho > \rho_+$ (see Figs. 8(a, b)).

For $\widetilde{q} > -0.63$ the NUP region is split into two independent regions, NUP (lower intensities) and NUP* (larger intensities), which are connected by an unstable UP1 solution as shown in Figure 8(c). Starting from the NUP (NUP*) solution and increasing (lowering) the intensity, the system eventually undergoes a discontinuous transition to UP2 state via a homoclinic bifurcation. The separation between NUP and NUP* regions increases when $\widetilde{q}$ is increased. Moreover the NUP* region shifts to higher intensities and its interval of existence becomes

smaller. At some critical $\widetilde{q}$, the UP1 state at higher intensities loses its stability at the saddle-node SN giving rise to a second NUP$^*$ region. Then, as $\widetilde{q}$ increases, such region develops towards lower values of $\rho$ as demonstrated in Figure 8(d) and the unstable UP1 states exist over a larger range of intensity (see the line $Hf_B$-SN in Fig. 8(d)). These NUP$^*$ regions eventually merge into a single one, but a stable UP1 island (see the line A-B in Fig. 8(e)) still exists. At larger $\widetilde{q}$, this island disappears and finally, at $\widetilde{q} = -0.25$, the NUP$^*$ region shrinks to zero. For $\widetilde{q} > -0.25$ the situation becomes qualitatively similar to the case of a pure nematic (Fig. 8(f)) until the value $\widetilde{q} = \widetilde{q}_2$ is reached, where the NUP state completely disappears (Fig. 3(d)).

It is worth noting that the scenarios depicted in Figures 8(a, b) might be experimentally realized. One should recall that they are qualitatively different from the ones obtained in the pure nematic case as shown in Figure 8(f). Indeed, in the former case (with intensity increasing) one deals with a continuous NUP → UP1 transition whereas in the latter case there is a discontinuous NUP → UP2 transition. However, the experimental demonstration of scenarios shown in Figures 8(c–e) may be difficult. Namely, the NUP$^*$ regime (for $-0.63 < \widetilde{q} < -0.25$) cannot be reached by slow increase of the light intensity. Indeed, the first NUP regime is always followed by a discontinuous transition via a homoclinic bifurcation to a UP2 state. We have checked the possibility to reach either the NUP$^*$ states or the stable UP1 island by an abrupt increase of the intensity starting from stable states lying at lower intensities (*i.e.* homeotropic, UP1 or NUP states) but the result was negative. A possible experimental realization might be the following, starting with a value of $\widetilde{q}$ that corresponds to the scenario shown in Figure 8(b), just before the NUP region splits into two distinct regions (see Fig. 8(c)). Then, one smoothly (to avoid transient fluctuations that could initiate an abrupt, and irreversible, jump to a UP2 state) increases the intensity starting from the unperturbed state to approach the UP1 states occurring after the NUP region (*i.e.* $\rho \simeq \rho_+$). Finally, the temperature of the system should be changed in such a way that the value of $\widetilde{q}$ is increased. We speculate that using this method one can reach the family of stable solutions at higher intensities (see Figs. 8(c–e)). In that case, a further exploring of the bifurcation diagram becomes possible by smooth change of the intensity (at fixed temperature).

## 5 Conclusion

The optical reorientation induced by circularly polarized light in homeotropically aligned long-pitch cholesteric films, *i.e.* chirally doped nematic films, has been studied theoretically. The key parameter used in our study is the (dimensionless) wave vector $\widetilde{q} = qL/\pi$ that describes the intrinsic helical structure, where $q = 2\pi/P$, $P$ is the cholesteric pitch and $L$ is the cell thickness. As is known, the bulk homeotropic orientation (without illumination) is stable only below the threshold value $|\widetilde{q}| = \widetilde{q}^*$ (typically $\widetilde{q}^* \sim$ 2–3), above which domains appear in spatially extended systems. In our case, however, the chiral dopant concentration is small ($|\widetilde{q}| < \widetilde{q}^*$) and the initial homeotropic orientation is destabilized by light above an intensity threshold that is reduced in comparison with the case without chiral dopant. We note that the cell thicknesses used in optically induced reorientation experiments (at visible wavelength) are typically of the order of 100 $\mu$m, any experimental realization thus deals with long-pitch cholesterics since $|\widetilde{q}| < \widetilde{q}^*$ corresponds typically to $P$ larger than $L$. We have evaluated quantitatively the role of the cholesteric pitch on the light-induced reorientation dynamics. The experimental counterpart can be done by adjusting the amount of chiral molecules added to a nematic sample. We have shown that the bifurcation scenario is significantly affected by the presence of chiral agents which introduce internal twist deformation in the medium and compared it with the pure nematic case ($\widetilde{q} = 0$). This is an additional confirmation of the essential role played by twist deformations in optically induced reorientation dynamics of liquid crystals, which is well known in the case of pure nematics. The main results of the present study are summarized in what follows. The optical Fréedericksz transition is found to be continuous if $q < \widetilde{q}_c$ and discontinuous in the opposite case. The critical value $q_c$ turns out to be small and for the present situation it is $\widetilde{q}_c \sim 5.8 \times 10^{-3}$. In addition, an optical bistability is predicted in the vicinity of the supercritical optical Fréedericksz transition for small values of $|\widetilde{q}|$ which has not yet been confirmed by existing experimental observations. While an approximate model is able to describe qualitatively the behavior of the system in the neighborhood of the optical Fréedericksz transition, rigorous simulations are necessary for a proper understanding of all phenomena. Theoretical predictions shed light on previous experiments and give a detailed picture of how the reorientation processes are affected when the chiral parameter is changed. In particular, the optical bistability between a slightly and a largely reoriented precessing state has been fully described and its all-optical analog (without chiral dopant) has been discussed. It turns out that the optical bistability extends over a large range of intensities only when the helicity of the circularly polarized light is the same as the one of the material and our findings agree qualitatively with known experimental results. This has led us to an interpretation in terms of a competition between an intrinsic spatial helical pattern (due to the chiral dopant) and an extrinsic one (due to the light) that can have either the same or opposite chirality. We have also found that the dynamical regime consisting of a non-uniform precession of the director around the light propagation axis, when $\widetilde{q} = 0$, is suppressed for large enough values of $|\widetilde{q}|$, which is confirmed by available experimental data. The mechanism of disappearance has nevertheless been shown to depend on the sign of $\widetilde{q}$. In particular, a new family of uniformly and non-uniformly precessing states at higher intensities, which do not exist in the pure nematic case, has been found for $\widetilde{q} < 0$. The possible experimental observation of such states has been proposed.

Financial support by the Deutsche Forschungsgemeinschaft under Kr 690/16-2 is gratefully acknowledged.

## References


1. P.G. de Gennes, J. Prost, *The Physics of Liquid Crystals*, 2nd edition (Clarendon Press, Oxford, 1993).
2. W.E.L. Hass, J.E. Adams, Appl. Phys. Lett. **25**, 535 (1974).
3. V.G. Bhide, S.C. Jain, S. Chandra, J. Appl. Phys. **48**, 3349 (1977).
4. G. Abbate, P. Maddalena, L. Marrucci, L. Saetta, A. Ferraiuolo, E. Santamato, Mol. Cryst. Liq. Cryst. **223**, 11 (1992).
5. G. Abbate, A. Ferraiuolo, P. Maddalena, L. Marrucci, E. Santamato, Liq. Cryst. **14**, 1431 (1993).
6. P. Maddalena, G. Arnone, G. Abbate, L. Marrucci, E. Santamato, Mol. Cryst. Liq. Cryst. **261**, 113 (1995).
7. E. Brasselet, T.V. Galstian, Opt. Commun. **200**, 241 (2001).
8. E. Santamato, B. Daino, M. Romagnoli, M. Settembre, Y.R. Shen, Phys. Rev. Lett. **57**, 2423 (1986).
9. E. Brasselet, T.V. Galstian, L.J. Dubé, D.O. Krimer, L. Kramer, J. Opt. Soc. Am. B **22**, 1671 (2005) .
10. L. Marrucci, G. Abbate, S. Ferraiuolo, P. Maddalena, E. Santamato, Phys. Rev. A **46**, 4859 (1992).
11. A. Vella, B. Piccirillo, E. Santamato, Phys. Rev. E **65**, 031706 (2002).
12. Refractive indices measured at 20 °C and $\lambda = 589$ nm from Merck datasheet.
13. G. Cipparrone, D. Duca, C. Versace, C. Umeton, N.V. Tabiryan, Mol. Cryst. Liq. Cryst. Sci. Technol. A **266**, 263 (1995).
14. B.Y. Zel'dovich, N. Tabiryan, Zh. Eksp. Teor. Fiz. **82**, 1126 (1982) (Sov. Phys. JETP **56**, 563 (1982)).
15. D.O. Krimer, G. Demeter, L. Kramer, Mol. Cryst. Liq. Cryst. **421**, 117 (2004).
16. E. Brasselet, T.V. Galstian, Opt. Commun. **186**, 291 (2000).